THE JOURNAL OF
Obstetrics and Gynaecology Research

doi:10.1111/jog.12136 J. Obstet. Gynaecol. Res. Vol. 40, No. 1: 263–267, January 2014

Humoral hypercalcemia caused by uterine corpus carcinosarcoma consisting of squamous cell carcinoma in its epithelial component

Shiro Takamatsu[1], Noriomi Matsumura[1], Tsukasa Baba[1], Masaki Mandai[1], Yoshiki Mikami[2] and Ikuo Konishi[1]

Departments of [1]Gynecology and Obstetrics and [2]Pathology, Kyoto University Graduate School of Medicine, Kyoto, Japan

Abstract

Humoral hypercalcemia of malignancy (HHM) is a paraneoplastic syndrome primarily caused by a tumor-producing parathyroid hormone-related protein (PTH-rP). We describe the first reported case of a uterine carcinosarcoma causing HHM. A 70-year-old patient was transferred to our hospital for a uterine tumor accompanied by impaired consciousness. The laboratory tests indicated anemia, malnutrition, elevated serum calcium and elevated PTH-rP. Emergency surgery, including abdominal hysterectomy and bilateral salpingo-oophorectomy, was performed due to uncontrollable uterine bleeding. The pathological diagnosis was carcinosarcoma consisting of pure squamous cell carcinoma in its epithelial component. Postoperatively, chemotherapy with paclitaxel and carboplatin was performed. The patient had recurrent tumors at the para-aortic lymph nodes 11 months after the initial surgery and underwent a pelvic and para-aortic lymphadenectomy, which removed all of the recurrent tumors.

Key words: carcinosarcoma, hypercalcemia, parathyroid hormone-related protein, squamous cell carcinoma, uterine neoplasms.

Introduction

We report a rare case of uterine carcinosarcoma with pure squamous cell carcinoma (SCC) in its epithelial component. This tumor caused humoral hypercalcemia of malignancy (HHM) by secreting parathyroid hormone-related protein (PTH-rP). This report suggests that HHM should be included in the list of differential diagnoses when a patient with SCC has a consciousness disorder regardless of the primary site as SCC is closely linked to PTH-rP.[1]

Case Report

A 70-year-old Japanese woman with a habit of smoking and drinking, menopause at age 51 years and a history of two cesarean sections was transferred to the Kyoto University Hospital for the treatment of a uterine tumor. She presented a 1-year history of brownish vaginal discharge; a 6-month history of gradually worsening polyarthralgia, fatigue, lethargy and anoxia; and a 5-kg weight loss. She initially visited the orthopedics department for rheumatoid arthritis (RA), where the abdominal mass was found. At that time, her general condition became worse and her level of consciousness declined.

The initial physical examination at our hospital revealed a mild consciousness disorder and anemic conjunctiva. The pelvic examination revealed purulent vaginal discharge and a newborn-head-sized uterus. The laboratory tests (Table 1) demonstrated anemia (decreased hemoglobin), malnutrition (decreased

Received: November 7 2012.
Accepted: March 25 2013.
Reprint request to: Dr Noriomi Matsumura, 54 Shogoin Kawahara-cho, Sakyo-ku, Kyoto 606-8507, Japan. Email: noriomi@kuhp.kyoto-u.ac.jp
Conflict of interest: The authors have no conflict of interest.

Table 1 Laboratory tests

Laboratory tests	Normal range	Day 1	Day 21	Day 42	Day 142	Day 350	Day 418
Hemoglobin (g/dL)	10.2–14.6	6.9	8.9	10.2	8.7	10.4	9.6
Albumin (g/dL)	3.9–5.1	2.0	2.8	4.1	3.9	3.5	3.7
C-reactive protein (mg/dL)	<0.2	23.4	2.0	1.6	0.1	3.2	0.6
Creatinine (mg/dL)	0.4–0.8	1.0	0.5	0.5	0.6	0.7	0.6
Calcium (mg/dL)†	8.5–9.9	14.2	8.9	8.7	9.2	9.1	—
Intact PTH (pg/mL)	10–65	<5	57	—	47	40	45
PTH-rP (pmol/L)	<1.1	4	<1.1	—	<1.1	1.1	<1.1
$1,25(OH)_2D_3$ (pg/mL)	20–60	13	50	—	41	44	44
CA125 (U/mL)	<35	160	—	19.7	10.7	9.6	—
SCC (ng/mL)	<1.5	3.4	—	0.7	1.0	1.1	0.7
Rheumatoid factor (IU/mL)	<11.7	28.3	—	30.8	<8.0	<8.0	<8.0

Day 1 indicates the date of the first admission. The initial surgery was performed on day 9 and the second surgery on day 358. Chemotherapy was performed from days 52–219. '—' indicates no data. †Corrected calcium level based on the albumin level. CA125, carbohydrate antigen 125; PTH-rP, parathyroid hormone-related protein; SCC, squamous cell carcinoma.

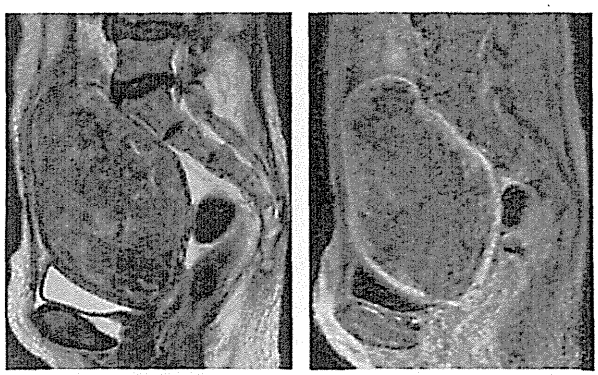

Figure 1 Pelvic magnetic resonance images (left, T_2; right, gadolinium-enhanced T_1-weighted image). A bulky uterine tumor with heterogeneous intensity fully occupied the uterine cavity.

albumin), inflammatory status (increased C-reactive protein) and a slight kidney disorder (increased creatinine). Furthermore, consistent with HHM, severe hypercalcemia, elevated PTH-rP, decreased $1,25(OH)_2D_3$ and decreased intact PTH were detected. The calcium level (14.2 mg/dL) suggested that the consciousness disorder was caused by HHM. Tumor markers (carbohydrate antigen 125 and SCC) were elevated, implying the existence of malignant tumors. An endometrial biopsy indicated high-grade carcinoma. Pelvic magnetic resonance images demonstrated a bulky uterine tumor that fully occupied the uterine cavity (Fig. 1). Neither lymphadenopathy nor extrauterine metastases were found by computed tomography.

After hospitalization, the patient was treated by massive hydration, diuresis and bisphosphonate to normalize the serum calcium level. Fatigue, anorexia and polyarthralgia were improved. RA was treated with oral salazosulfapyridine and prednisolone, which relieved its symptoms. However, the anemic, malnourished and hyperinflammatory status continued, and on the 8th hospital day, when she presented massive genital bleeding, hemoglobin levels decreased to 6.1 g/dL. Therefore, an emergency total hysterectomy with bilateral salpingo-oophorectomy was performed to stop the bleeding and the tumor-associated endocrinal abnormalities.

Grossly, the uterine tumor measured 15 cm in greatest dimension and its cut surface was pinkish or yellowish, with extensive necrosis (Fig. 2a). A microscopic examination revealed a mixture of high-grade SCC (Fig. 2b,c) and sarcomatous components composed of atypical spindle-shaped cells without evidence of specific differentiation. This component was well demarcated from carcinomatous components (Fig. 2c). In addition, metaplastic squamous epithelium overlying pre-existing endometrium was identified adjacent to the tumor (Fig. 2d). The invasion extended to the full thickness of the myometrium, with much lymphovascular invasion. The uterine cervix was intact. Immunohistochemically, the carcinomatous components were positive for cytokeratin 5 and p63 (Fig. 2e, f), and negative for cytokeratin 7, estrogen receptor and progesterone receptor. The sarcomatous components were positive for vimentin (Fig. 2g) and negative for cytokeratin. Both components were positive for p53

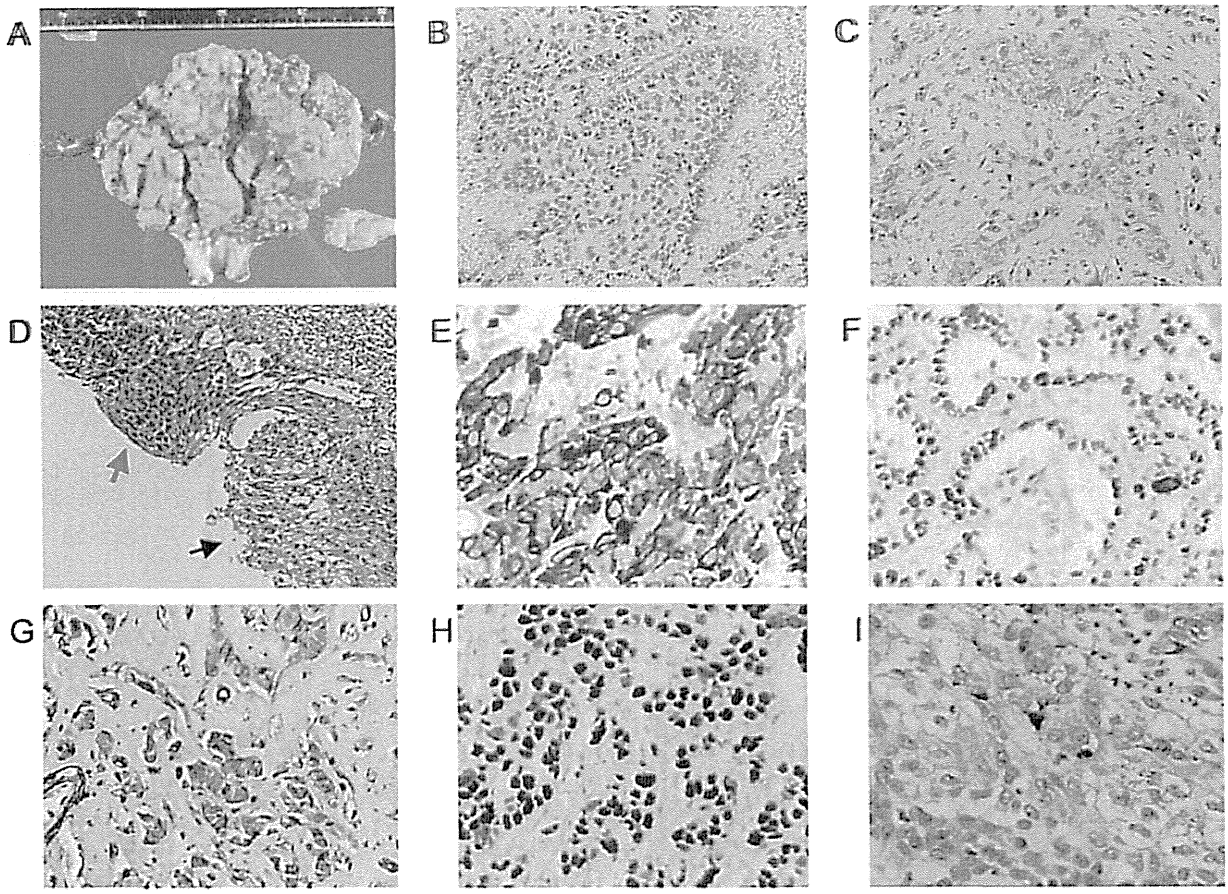

Figure 2 Pathological findings of the tumor. (a) Gross examination. (b–d) Microscopic examination (×200). (b) The epithelial components consisted of high-grade squamous cell carcinoma with keratinizing tendency. (c) The mesenchymal cells surrounding the epithelial cells consisted of atypical spindle-shaped tumor cells. (d) A squamous metaplasia (red arrow) existed adjacent to the squamous cell carcinoma (black arrow). (e–i) Immunohistochemical examination (×400). The epithelial components were positive for cytokeratin 5 (e) and p63 (f). The sarcomatous components were positive for vimentin (g). Both components were positive for p53 (h) and parathyroid hormone-related protein (i).

and PTH-rP (Fig. 2h, i). Based on these findings, the pathological diagnosis of carcinosarcoma of homologous type was established, which was considered to be associated with ichthyosis uteri. The postoperative stage was IB (International Federation of Gynecology and Obstetrics 2008).

Postoperatively, the serum PTH-rP and intact PTH levels were promptly normalized (Table 1), and the general condition was markedly improved. However, the elevated rheumatoid factor (RF) was not normalized, and the oral medication against RF was therefore continued. One month after the surgery, the patient received chemotherapy with paclitaxel (180 mg/m^2) and carboplatin (area under the curve, 6.0), which was repeated every 4 weeks for 6 months. The patient had recurrent tumors at the para-aortic lymph nodes 11 months after the initial surgery. At that time, PTH-rP was just over the cut-off (1.1 pmol/L, Table 1). She received pelvic and para-aortic lymphadenectomy, which removed all the recurrent tumors. The histopathological examination revealed pure SCC in the para-aortic lymph nodes. Currently, 2 months after the secondary surgery, there is no recurrent disease.

Discussion

Uterine carcinosarcomas, rare entities accounting for only 1–2% of uterine neoplasms, usually occur in elderly postmenopausal women. Histopathologically, they contain both epithelial and mesenchymal elements. It is believed that in most cases, both components arise from a monoclonal epithelial cell that is capable of multilineage differentiation, resulting in sarcomatous metaplasia.[2] As the carcinomatous component, serous adenocarcinoma is the most common, and pure SCC has been reported in only four cases.[3–5] The differential diagnoses of SCC in the endometrium are squamous metaplasia from endometrioid adenocarcinoma and endometrial invasion of SCC from the uterine cervix. In our case, neither endometrioid adenocarcinoma nor cervical carcinoma was found by a thorough examination of the subject. According to the metaplasia theory, the carcinosarcoma in our case might have been generated from a malignant squamous cell in the endometrium. A strong association between SCC and chronic inflammation in the endometrium, such as pyometra, has been reported,[6] although this condition was not diagnosed in our case before diagnosis of the tumor. Consistent with previous reports on the coexistence of squamous metaplasia and SCC,[7] squamous metaplasia existed adjacent to the malignant epithelium in our case (Fig. 2d), suggesting that this lesion could be the precancerous lesion.

Hypercalcemia occurs in approximately 20–30% of malignancies.[8] Tumor secretion of PTH-rP, referred to as HHM, is found in up to 80% of patients with hypercalcemia of malignancy. Although a wide variety of malignancies can be associated with HHM, SCC in the lung, head and neck are the most common, accounting for 50% of all HHM cases. This prevalence is reasonable because PTH-rP is closely associated with keratinocyte differentiation and maturation, and almost 100% of SCC are positive for PTH-rP expression regardless of their tissue origins.[1] There have been only nine reported cases of uterine corpus malignant tumors that caused HHM,[9–13] and our case is the first reported case of uterine carcinosarcoma that caused HHM. This rarity is most likely attributable to the rarity of SCC in the endometrium.

Because uterine carcinosarcomas are highly aggressive with a poor prognosis, it is believed that lymphadenectomy could improve the prognosis of this disease.[14] However, in our case, we had to perform an emergency surgery in the presence of severe anemia and malnutrition and were unable to conduct a lymphadenectomy. Given the pattern of recurrence, with tumors only at para-aortic lymph nodes, lymphadenectomy would be beneficial to prevent recurrence. We used a combination of paclitaxel and carboplatin as adjuvant chemotherapy because it is one of the most effective regimens against carcinosarcoma.[15] However, the patient had a recurrent tumor soon after the end of chemotherapy, indicating that this regimen was not effective. Reports on the treatment of endometrial SCC are scarce. Further studies, including case reports, are necessary to optimize the treatment of this rare disease.

In summary, this case report shows that uterine corpus carcinosarcoma containing SCC in its epithelial component can cause HHM. This condition seems to be extremely rare but suggests a reasonable pathogenesis for endometrial malignancies.

References

1. Dunne FP, Lee S, Ratcliffe WA, Hutchesson AC, Bundred NJ, Heath DA. Parathyroid hormone-related protein (PTHrP) gene expression in solid tumours associated with normocalcaemia and hypercalcaemia. *J Pathol* 1993; **171**: 215–221.
2. McCluggage WG. Malignant biphasic uterine tumours: Carcinosarcomas or metaplastic carcinomas? *J Clin Pathol* 2002; **55**: 321–325.
3. Norris HJ, Taylor HB. Mesenchymal tumors of the uterus. 3. A clinical and pathologic study of 31 carcinosarcomas. *Cancer* 1966; **19**: 1459–1465.
4. Iwasa Y, Haga H, Konishi I *et al.* Prognostic factors in uterine carcinosarcoma: A clinicopathologic study of 25 patients. *Cancer* 1998; **82**: 512–519.
5. Szukala SA, Marks JR, Burchette JL, Elbendary AA, Krigman HR. Co-expression of p53 by epithelial and stromal elements in carcinosarcoma of the female genital tract: An immunohistochemical study of 19 cases. *Int J Gynecol Cancer* 1999; **9**: 131–136.
6. Goodman A, Zukerberg LR, Rice LW, Fuller AF, Young RH, Scully RE. Squamous cell carcinoma of the endometrium: A report of eight cases and a review of the literature. *Gynecol Oncol* 1996; **61**: 54–60.
7. Zidi YS, Bouraoui S, Atallah K, Kchir N, Haouet S. Primary in situ squamous cell carcinoma of the endometrium, with extensive squamous metaplasia and dysplasia. *Gynecol Oncol* 2003; **88**: 444–446.
8. Stewart AF. Clinical practice. Hypercalcemia associated with cancer. *N Engl J Med* 2005; **27**: 373–379.
9. Sachmechi I, Kalra J, Molho L, Chawla K. Paraneoplastic hypercalcemia associated with uterine papillary serous carcinoma. *Gynecol Oncol* 1995; **58**: 378–382.
10. Tang SJ, Geevarghese S, Saab S *et al.* A parathyroid hormone-related protein-secreting metastatic epithelioid leiomyosarcoma. A case report and review of the literature. *Arch Pathol Lab Med* 2003; **127**: e181–e185.
11. Kinugasa Y, Morishige K, Kamiura S, Tsukamoto Y, Saji F. Parathyroid hormone-related protein-secreting uterine endometrioid adenocarcinoma. *Jpn J Clin Oncol* 2006; **36**: 113–115.

12. Pinal-Fernández I. Humoral hypercalcemia in mixed endometrial carcinoma. *An Sist Sanit Navar* 2010; 33: 217–219.
13. Richey DS, Welch BJ. Concurrent primary hyperparathyroidism and humoral hypercalcemia of malignancy in a patient with clear cell endometrial cancer. *South Med J* 2008; 101: 1266–1268.
14. Temkin SM, Hellmann M, Lee YC, Abulafia O. Early-stage carcinosarcoma of the uterus: The significance of lymph node count. *Int J Gynecol Cancer* 2007; 17: 215–219.
15. Toyoshima M, Akahira J, Matsunaga G *et al*. Clinical experience with combination paclitaxel and carboplatin therapy for advanced or recurrent carcinosarcoma of the uterus. *Gynecol Oncol* 2004; 94: 774–778.

Oxford Journals > Medicine & HealthScience & Mathematics > Carcinogenesis > Volume 35 Issue 4 > Pp. 760-768.

Identification of KLF17 as a novel epithelial to mesenchymal transition inducer via direct activation of TWIST1 in endometrioid endometrial cancer

Peixin Dong[1,*,†], Masanori Kaneuchi[1,†], Ying Xiong[2], Liping Cao[2], Muyan Cai[3], Xishi Liu[4], Sun-Wei Guo[5], Jingfang Ju[6], Nan Jia[7,9], Yosuke Konno[8], Hidemichi Watari[8], Masayoshi Hosaka[8], Satoko Sudo[8] and Noriaki Sakuragi[1,8]

[1] Department of Women's Health Educational System, Hokkaido University School of Medicine, Hokkaido University, Sapporo 0608638, Japan,

[2] Department of Gynecology, State Key Laboratory of Oncology in South China, Sun Yat-sen University Cancer Center, Guangzhou 510060, P. R. China,

[3] Department of Pathology, State Key Laboratory of Oncology in South China, Sun Yat-sen University Cancer Center, Guangzhou 510060, P. R. China,

[4] Shanghai OB/GYN Hospital, Fudan University, Shanghai 200011, P. R. China,

[5] Shanghai Key Laboratory of Female Reproductive Endocrine Related Diseases, Shanghai 200011, P. R. China,

[6] Department of Pathology, Stony Brook Medicine, Stony Brook University, NY 11794–8691, USA,

[7] Ruijin Hospital, Shanghai Institute of Hypertension, Shanghai Jiao Tong University Medical School, Shangai 200025, P. R. China and

[8] Department of Gynecology, Hokkaido University School of Medicine, Hokkaido University, Sapporo 0608638, Japan

[9] Present address: Department of Cardiology, the Fourth People's Hospital of Shenzhen, Shenzhen, 518033, P. R. China.

*To whom correspondence should be addressed. Tel: +81 11 706 5941; Fax: +81 11 706 7711; Email: dpx1cn{at}gmail.com
Correspondence may also be addressed to Ying Xiong. Tel: +86 20 87343101; Fax: +86 20 87343014; Email: tdken999{at}163.com
†These authors contributed equally to this work.

Received May 29, 2013.
Revision received October 2, 2013.
Accepted October 26, 2013.

Abstract

Krüppel-like factor 17 (KLF17), a member of the KLF transcription factor family, has been shown to inhibit the epithelial–mesenchymal transition (EMT) and tumor growth. However, the expression, the cellular function and the mechanism of KLF17 in endometrioid endometrial cancer (EEC; a dominant type of endometrial cancer) remain elusive. Here, we report that among the KLF family members, KLF17 was consistently upregulated in EEC cell lines compared with immortalized endometrial epithelial cells. Overexpression of KLF17 in EEC cell lines induced EMT and promoted cell invasion and drug resistance, resulting in increased expression of TWIST1. In contrast, KLF17 suppression reversed EMT, diminished cell invasion, restored drug sensitivity and suppressed TWIST1 expression. Luciferase assays, site-directed mutagenesis and transcription factor DNA-binding analysis demonstrated that KLF17 transactivates TWIST1 expression by directly binding to the TWIST1 promoter. Knockdown of TWIST1 prevented KLF17-induced EMT. Consistent with these results, both KLF17 and TWIST1 levels were found to be elevated in EECs compared with normal tissues. KLF17 expression positively correlated with tumor grade but inversely correlated with estrogen and progesterone receptor expression. Thus, KLF17 may have an oncogenic role during EEC progression via initiating EMT through the regulation of TWIST1.

Introduction

Endometrial cancer is the most common type of gynecological cancer among women in the USA (1), with a rapidly increasing incidence in Japan (2). The majority of endometrial cancers (over 80%) is well differentiated with endometrioid [endometrioid endometrial cancer (EEC)] histology, diagnosed at an early stage, and entails a favorable survival rate (3). However, EEC patients who display an advanced stage disease or suffer a metastatic recurrence have an extremely poor prognosis with a median survival of ~7–10 months (4).

EECs often express estrogen receptor (ER) and progesterone receptor (PR) and exhibit a high rate of *PTEN* tumor-suppressor gene loss or mutation (4). Epithelial–mesenchymal transition (EMT) is a biological process in which epithelial cells lose basal–apical polarity, become more spindle shaped and acquire the motile and cancer stem cell (CSC) phenotypes with a heightened propensity to metastasize to distant organs (5). TWIST1 has been shown to promote EMT in human cancer, by either directly repressing epithelial marker E-cadherin (6) or upregulating the expression of the EMT inducer BMI-1, which binds the E-cadherin promoter and suppresses its transcription (7,8). We recently characterized the oncogenic roles of TWIST1 and BMI-1 in inducing EMT in EEC cells (9,10). However, the mechanisms that mediate TWIST1 expression during EEC metastasis remain largely unknown.

The Krüppel-like factor (KLF) transcription factor family proteins (1–17) play important roles in a variety of physiological and oncogenic processes, including tumor growth and metastasis. A number of KLFs can influence transcriptional networks involved in the control of cancer cell invasion (11), apoptosis (11), proliferation (12) and the maintenance of CSC (13). In endometrial cancers, the transcript levels of KLF9 were downregulated, and the levels of KLF13 were upregulated relative to normal endometrium (14). Furthermore, KLF17 has been reported to serve as an inhibitor of EMT and metastasis in breast cancer (15), and reduced expression of KL17 is associated with poor prognosis in lung cancer and liver cancers (16,17). However, the expressions, molecular roles and the underlying mechanisms of KLF gene family members during the progression of EEC remain to be elucidated.

Here, we report that KLF17 is overexpressed in human EECs relative to normal endometrium and that upregulation of KLF17 is sufficient to induce EMT and invasive phenotypes of EEC cells. Our results demonstrate that KLF17 directly binds the TWIST1 promoter to transactivate TWIST1. Taken together, these results suggest that KLF17 may play an oncogenic role in metastatic EEC, with TWIST1 as a major downstream target.

Materials and methods

Cell lines and culture

The Ishikawa and HHUA EEC cell lines are ER and PR-positive, grade 1 tumor cells with PTEN mutations (18). Ishikawa cells were obtained from the American Type Culture Collection (ATCC, Manassas, VA), and HHUA cells were purchased from the RIKEN cell bank (Tsukuba, Japan). Cells were cultured in Dulbecco's modified Eagle's medium/F12 medium (Sigma–Aldrich, St Louis, MO) supplemented with 15% fetal bovine serum. The immortalized human endometrial epithelial cell line EM [ER/PR-positive, wild-type PTEN (19,20)] was kindly provided by Professor Satoru Kyo (Kanazawa University, Ishikawa, Japan) and maintained in Dulbecco's modified Eagle's medium/F12 medium supplemented with 15% fetal bovine serum.

Stable overexpression of KLF17 in Ishikawa cells

KLF17 complementary DNA (cDNA) in an expression vector was purchased from OriGene Technologies (Rockville, MD). Ishikawa cells were stably transfected as described previously (21). In brief, upon reaching 80% confluence, cells were transfected with Lipofectamine PLUS Reagent (Invitrogen, Carlsbad, CA) according to the manufacturer's protocols. Cells were selected in Dulbecco's modified Eagle's medium/F12 medium containing 0.5mg/ml G418 (Sigma–Aldrich, St Louis, MO) at 48h post-transfection. The selected polyclonal cells were then expanded.

Stable knockdown of KLF17 in HHUA cells

To produce the stable KLF17 knockdown cell line, we used the KLF17-expressing EEC cell line HHUA. The knockdown experiment was performed using KLF17 short-hairpin RNA (shRNA) lentiviral plasmids (Santa Cruz Biotechnology, Santa Cruz, CA). As a control, HHUA cells infected with a control shRNA were used. Transfected cells were selected using 1 μg/ml puromycin (Sigma–Aldrich, St Louis, MO). Three single colonies (C2, C4 and C5) expressing KLF17 shRNA constructs and two single colonies transduced with control shRNA vectors (shCtr1 and 2) were selected 4 weeks following transfection. Both shCtr1 and shCtr2 cells expressed comparable levels of KLF17, and shCtr1 cells were subsequently selected for use as shCtr control cells.

Transient transfection

Ishikawa and HHUA cells were transfected with either KLF17 cDNA vector (or control vector) or TWIST1 small interfering RNA (siRNA) (or control siRNA) from Ambion (Austin, TX), using Lipofectamine 2000 (Invitrogen, Carlsbad, CA) as indicated. After 48 h, cells were used for protein extraction or cell invasion assay.

Quantitative morphometric analysis

Quantitative morphometric analysis was performed as reported previously (22). In brief, the major and minor cell axis was outlined using LSM Image Browser software (Carl Zeiss). The ratio between the major axis and the minor axis of cells (morphological index) was calculated to determine the degree of elongated cell morphology. This ratio is higher in cells with long and thin extensions.

Western blot analysis

Whole cell lysates were obtained using the M-Per Mammalian Protein Extraction Reagent (Pierce Biotechnology, Woburn, MA). Nuclear protein extracts were prepared using a Nuclear Extraction Kit (Chemicon International, Temecula, CA) according to the manufacturer's instructions. Proteins (40 μg) were separated on 10% sodium dodecyl sulfate–polyacrylamide gel electrophoresis and transferred to nitrocellulose membranes. Antigen–antibody complexes were detected using the enhanced chemiluminescence blotting analysis system (Amersham Pharmacia Biotech, Buckinghamshire, UK). The following antibodies were used for analysis: rabbit polyclonal anti-KLF17 (ab84196, Abcam, Cambridge, UK), mouse monoclonal anti-Twist (ab50887, Abcam), mouse monoclonal anti-GAPDH (sc-47724, Santa Cruz Biotechnology, Santa Cruz, CA), rabbit polyclonal anti-BMI-1 (ab38295, Abcam), rabbit polyclonal anti-E-cadherin (A01589, GenScript, Edison, NJ), mouse monoclonal anti-PARP-1 (Santa Cruz Biotechnology), mouse monoclonal anti-paxillin (Santa Cruz Biotechnology) and rabbit polyclonal anti-Vimentin (A01189, GenScript, Edison, NJ). Primary and secondary antibodies were used at 1:1000–2000 and 1:5000 dilutions, respectively. Immunoblot images were digitized and quantified using the NIH Image software.

In vitro cell invasion assay

At 24 h post-transfection, EEC cells (1×10^5) in 500 µl serum-free medium were added to the upper chamber of a transwell plate and 750 µl medium supplemented with 15% fetal bovine serum was added to the lower chamber, as described previously (23). Cells were allowed to migrate through the intermediate membrane for 24 h at 37°C. Membranes were then fixed with 10% formalin and stained in 1% toluidine blue solution. Cells attached to the lower side of the membrane were counted under a microscope in 10 high-power (×200) fields. Assays were performed in triplicate for each experiment with each experiment repeated three times.

Cell viability assay and proliferation assay

Cells (5×10^3) were plated in 96-well plates for 24 h and then treated with dimethyl sulfoxide or varying doses of paclitaxel (Cell Signaling Technology, Beverly, MA), at 10, 20 and 30nM. Cell viability was determined by the Cell Counting Kit-8 (Dojindo, Kumamoto, Japan) 24h later. The absorbance was determined at 450nm using a microplate reader, and the percentage absorbance was calculated against dimethyl-sulfoxide-treated cells. Cells (5×10^3) were plated in 96-well plates. After treatment with various concentrations of paclitaxel (3nM for Ishikawa cells and 1nM for HHUA cells), the growth curve of cells, covering a total of four days of culturing, was plotted with the Cell Counting Kit-8 method.

Colony formation assay

Approximately 1000 cells were added to each well of a six-well culture plate, and each experiment was performed in triplicate. After 12 days of culture at 37°C, cells were fixed with 10% formalin and stained with 10% Giemsa solution. The number of colonies containing ≥50 cells was counted under a microscope.

Real-time quantitative reverse transcription–polymerase chain reaction

Total RNA was isolated using TRIZOL reagent (Invitrogen, Carlsbad, CA) and reverse-transcribed using a Takara PrimeScript RT reagent kit (Takara, Shiga, Japan). Quantitative reverse transcription–polymerase chain reaction (qRT–PCR) was performed with the Applied Biosystems 7300 real-time PCR system (Applied Biosystems) using the Takara SYBR Premix Ex Taq II (Takara, Japan). Primers for *KLF* family genes except those amplifying *KLF*s (1, 8, 9, 13 and 14) were reported previously (24). Primers for *KLF*s (1, 8, 9, 13, 14 and 17), *TWIST1*, *ZEB1*, *BMI-1*, *Snail*, *Slug*, *E-cadherin*, *CK-18*, *Vimentin*, *NANOG*, *SOX-2*, *CD133*, *MDR-1*, *MRP-1* and *GAPDH* were obtained from the PrimerBank database (http://pga.mgh.harvard.edu/primerbank/). Gel electrophoretic analysis of RT–PCR products confirmed that the primers amplified a single band with the expected size.

Molecular cloning of the TWIST1 promoter

A 1.9kb fragment of the *TWIST1* gene 5′-regulatory region (–2068 to –159 with respect to the translational start site) overlapping potential KLF17-binding sites was amplified from human genomic DNA (Takara, Shiga, Japan), using forward primer (5′-AT*ACGCGT*GATTTCTGCAGCCACGTTCT-3′, *MluI*) and reverse primer (5′-CG ***AGATCT*** TCGGGGTCTAACAATTCGTC-3′, ***BglII***). The amplified product was subcloned into MluI/BglII sites of the pGL3-basic plasmid (Promega, Madison, WI) to produce wild-type (WT) TWIST1 pro-Luc vectors. Correct insertion was confirmed by gel electrophoresis and DNA sequencing.

Site-directed mutagenesis

Computer-assisted transcription-factor-binding site analysis (TransFac) of regions upstream of the *TWIST1* promoter identified six consensus KLF17-binding sites (A: –1625 to –1621; B: –1370 to –1366; C: –1176 to –1172; D: –524 to –520; E: from nucleotide –509 to –505; F: –439 to –435) at +1 and –2027bp upstream of the start site of transcription. The WT TWIST1 pro-Luc vector was used to generate mutant constructs containing the TWIST1 promoter sequence with point mutations in the

potential KLF17-binding sites (CACCC→CGTTC) using a QuickChange site-directed mutagenesis kit (Stratagene, La Jolla, CA). The resulting constructs were named Mutant TWIST1 pro-Luc vectors.

Luciferase activity assay

The luciferase reporters (WT TWIST1 pro-Luc vector, mutant TWIST1 pro-Luc vector, pGL-3 basic control vector, 100ng) and the pRL-CMV vector (10ng, Promega, Madison, WI) were co-transfected with and without increasing doses of KLF17 expression vector (25 and 50ng) and control vector (50ng) or with increasing doses of KLF17 siRNA (10 and 20nM) and control siRNA (20nM) as indicated. At 48 h after transfection, the luciferase activity was measured using a dual-luciferase assay (Promega, Madison, WI).

KLF17 DNA-binding assay

DNA binding of KLF17 to the promoter of *TWIST1* in Ishikawa and HHUA cells was measured using the universal EZ-TFA transcription factor assay colorimetric kit (Upstate Biotechnology, Lake Placid, NY). Nuclear extracts (15 μg) were prepared and incubated with 2 μl of capture probe, 5'-biotinylated double-stranded oligonucleotides (5′-GGCGAGATGA GACAT*CACCC*ACTGTGTAGAAGCTG-3′) corresponding to the positions –454 to –419 of the *TWIST1* promoter harboring the consensus KLF17-binding site F. After 1 h incubation, the capture probe bound to KLF17 was immobilized on the streptavidin-coated plate, and unbound material was washed away. Plates were then incubated with KLF17 antibody (1:1000) and horseradish-peroxidase-conjugated secondary antibody (1:500). Horseradish peroxidase activity was measured colorimetrically at 450nm using a microplate reader. To confirm the DNA-binding specificity of KLF17, a non-biotinylated double-stranded oligonucleotide with the same sequence as the capture probe was used as the competitor probe to ensure specificity. Biotinylated oligonucleotides containing a mutated KLF17-binding site F (5′-GGCGAGATGAGACAT*CGTTC*ACTGTGTAGAAGCTG-3′) were used as negative control. A background control containing binding buffer and capture probe without cell lysate was used as an additional control. KLF17 DNA binding is expressed as fold change over background.

Clinical sample selection and immunohistochemistry analysis

The use of clinical samples for this study was approved by the Institutional Ethics Committee of The Cancer Center, Sun Yat-Sen University. Paraffin blocks containing formalin-fixed paraffin-embedded tissues were obtained from 90 patients with EEC. Normal endometrium was collected from 18 patients. In addition, 24 pairs of EEC samples and adjacent normal endometrial tissues were obtained for RNA extraction. The clinical and pathological characteristics of EEC patients were shown in Supplementary Table 1, available at *Carcinogenesis* Online.

The streptavidin-biotin peroxidase complex technique was used for staining. Briefly, following antigen retrieval, deparaffinized slides were incubated with anti-KLF17 (1:100, ab84196, Abcam, Cambridge, UK) antibody overnight at 4°C. To visualize the reaction, the sections were incubated with the horseradish-peroxidase-conjugated secondary antibody for 30min followed by diaminobenzidene substrate for 2min. After the nuclei had been stained with hematoxylin, the sections were mounted with neutral gum. Negative control experiments omitting either primary or secondary antibody were also performed.

Double-blinded analysis was performed to evaluate the immunostaining score (IRS) of KLF17 expression with patient outcome and tumor characteristics. Slides were scored for staining intensity and proportion of positive tumor cells as previously reported (25). The staining intensity score ranged from 0 (absent), 1 (weak), 2 (moderate) to 3 (strong). The positive tumor cells varied from 0 (<5%), 1 (5–25%), 2 (26–50%), 3 (51–75%) to 4 (76–100%). The IRS was calculated as the sum of staining intensity and positive tumor cells (range 0–7). A final IRS ≥ 5 was considered high expression (5–6: ++; 7: +++) and an IRS ≤ 4 were considered low expression (0–2: –; 3–4: +).

For the ER-alpha and PR assay, samples were incubated with anti-ER (clone H-150, Santa Cruz Biotechnology, Santa Cruz, CA) or anti-PR antibody (SP2, Lab Vision Corporation, Fremont, CA) for 1h at room temperature. Quantification of immunochemical ER and PR staining was scored in a minimum of 300 tumor cells showing nuclear reaction. Tumors with positive ER or PR nuclear staining in >10% of tumor cells were defined as ER or PR positive (26).

Statistical analysis

All experiments were performed in triplicate. For *in vitro* results, values represent mean ± standard deviation and were analyzed by Student's *t*-test. The Fisher's exact test was used to compare the categorical data. Significance was defined as $P < 0.05$.

Results

KLF17 is overexpressed in EEC cell lines

We first investigated the expression pattern of the KLF gene family in two EEC cell lines along with the immortalized human endometrial epithelial cell EM by qRT–PCR. The two EEC cell lines, Ishikawa and HHUA exhibit representative molecular characteristics of well-differentiated steroid hormone receptor-positive EEC (18), were selected for a comprehensive screening for expression of KLF members. The results confirmed messenger RNA (mRNA) expression of all KLF members in the two EEC cell lines and EM cells. The expression profile of the data represented as a color-coded scale illustrates that a subset of the *KLF*s (1, 4, 5, 10, 13, 16 and 17) were consistently and significantly upregulated in the EEC cell lines compared with EM cells (Figure 1A). The expression of the remaining *KLF*s (2, 7, 8, 9, 11, 12, 14 and 15) was consistently lower in EEC cell lines. We focused on the *KLF* member, *KLF17*, whose magnitude of increase in mRNA abundance was the largest among all KLF family members in EEC cells (Figure 1B). Semiquantitative western blot analysis indicated that KLF17 protein expression was also significantly increased in the EEC cells, with HHUA cells displaying higher levels of KLF17 protein compared with Ishikawa cells (Figure 1C).

View larger version:

- In this window
- In a new window

- Download as PowerPoint Slide

Fig. 1.

KLF17 is upregulated in EEC cell lines than in immortalized endometrial epithelial cell. (**A**) The color-coded scale depict differentially regulated KLF family genes (1–17) between EEC cell lines (Ishikawa and HHUA) and immortalized endometrial epithelial cell line EM, as determined by qRT–PCRs ($n = 3$). Red indicates significantly higher mRNA expression, whereas green indicates significantly lower mRNA expression in cancer cells compared with EM cells, respectively. The expression levels of KLF17 mRNA (**B**) and protein (**C**) relative to EM cells, as determined by qRT–PCRs ($n = 3$; $^{**}P < 0.01$, normalized to GAPDH) and semiquantitative western blot analysis.

KLF17 induces the invasive and EMT phenotype of EEC cells

To define whether KLF17 has a role in EEC invasion and progression, we generated a gain-of-function model. Ishikawa cells with relatively lower levels of KLF17 were used to overexpress KLF17. Ectopic expression of both KLF17 mRNA and protein levels (Figure 2A and B) resulted in a transition from a round, tightly packed morphology to a more scattered spindle-shaped mesenchymal appearance (Figure 2C, left panel). Quantitative morphometric analysis suggested that the morphological index representing the degree of elongated cell morphology was significantly increased in KLF17-overexpressing Ishikawa cells (Figure 2C, right panel). Overexpression of KLF17 cDNA strongly promoted cell invasion of these cells (Figure 2D). Consistent with these findings, ectopic expression of KLF17 in Ishikawa cells led to decreased expression of the epithelial marker E-cadherin and increased expression of the mesenchymal marker Vimentin (Figure 2B).

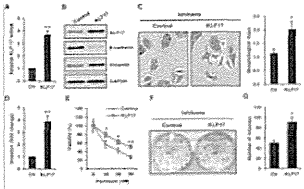

View larger version:

- In this window
- In a new window
- Download as PowerPoint Slide

Fig. 2.

KLF17 induces the invasive and EMT phenotype of EEC cells. Ishikawa cells were transfected with control (Ctr) vector or KLF17 expression vector. (**A**) The mRNA expression of KLF17 as analyzed by qRT–PCRs ($n = 3$; $^{**}P < 0.01$, normalized to GAPDH). (**B**) Total protein extracts from Ishikawa cells described in (A) were immunoblotted as indicated. (**C**) Ishikawa cells described in (**A**) were stained with toluidine blue, and quantitative analysis of cell morphology shows the scattered mesenchymal morphology induced by overexpression of KLF17. (**D**) Overexpression of KLF17 significantly promotes EEC cell invasion ($n = 3$, $^{**}P < 0.01$). (**E**) Ishikawa cells described in (**A**) were incubated with the indicated concentrations of paclitaxel for 24h and cell viability assay was performed ($n = 3$; $^{*}P < 0.05$; $^{**}P < 0.01$). (**F**) Enforced KLF17 expression increases the proliferation of Ishikawa cells. (**G**) Colony number was counted ($n = 3$; $^{*}P < 0.05$).

The induction of EMT has been shown to modulate the cancer stem-like cell properties and confer increased drug resistance of cancer cells (27). To determine whether KLF17 plays a role in mediating cellular sensitivity to cytotoxic drugs in EEC cells, we treated Ishikawa cells with increasing concentrations of paclitaxel for 24h and assessed the chemosensitizing properties of control and KLF17-transfected cells using the cell viability assay. We found that loss of cell viability upon exposure to paclitaxel was much more pronounced in Ishikawa cells transduced with empty vector than in cells transfected with KLF17 cDNA (Figure 2E). These data indicate that overexpression of KLF17 in EEC cells may confer resistance to paclitaxel treatment. Given that KL17 has been shown to inhibit proliferation of lung cancer (16), we used the clone formation assay to examine the effects of KLF17 overexpression on the proliferation of Ishikawa cells. Enforced expression of KLF17 in Ishikawa cells significantly increased the colony formation capacity (Figure 2F and G). Consistent with these results, overexpression of KLF17 resulted in increased cell proliferation and paclitaxel resistance in Ishikawa cells, as measured by the cell counting kit-8 assay (Supplementary Figure S1A, available at *Carcinogenesis* Online). Taken together, these data indicate that KLF17 upregulation is sufficient to induce EMT and promote EEC invasion and progression.

Loss of KLF17 inhibits cell invasion and reverts the EMT phenotype in EEC cells

To further confirm the association of KLF17 expression with cancer cell invasive and EMT features, we knocked down endogenous KLF17 in HHUA cells with high endogenous levels of KLF17 using lentivirus-driven shRNA constructs (Figure 3A and D). KLF17 knockdown changed cell morphology from a scattered pattern to more round, tightly packed colonies (Figure 3B, left panel). KLF17 knockdown in HHUA cells significantly reduced the morphological index compared with the control shRNA-transfected condition (Figure 3B, right panel). This effect was associated with reduced cell invasion (Figure 3C) and altered expression of reported EMT-related genes (6,8), including upregulation of epithelial marker E-cadherin, and downregulation of EMT inducer BMI-1 and mesenchymal marker Vimentin (Figure 3D). We next analyzed whether loss of KLF17 could modulate chemoresistance and cell proliferation of HHUA cells. Knockdown of KLF17 sensitized HHUA cells to paclitaxel and resulted in suppressed clone formation (Figure 3E and F). Similarly, the cell counting kit-8 assay shows that the transfection with KLF17 shRNA significantly inhibits cell proliferation and decreased resistance to paclitaxel treatment (Supplementary Figure S1B, available at *Carcinogenesis* Online). Collectively, these data suggest that the downregulation of KLF17 in HHUA cells results in attenuated cell invasion and also disruption of the EMT process.

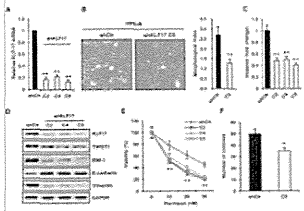

View larger version:

- In this window
- In a new window
- Download as PowerPoint Slide

Fig. 3.

KLF17 knockdown decreases cell invasion and reverts EMT phenotype in HHUA cells. (**A**) qRT–PCRs analysis for HHUA cells transfected with control shRNA (shCtr) vectors or KLF17 shRNA vector (single clone C2, 4 and 5; $n = 3$; $^{**}P < 0.01$, normalized to GAPDH. (**B**) Quantitative morphometric analysis shows that the shCtr cells exhibit a scattered morphology, whereas KLF17 shRNA-transfected cells show a more round, tightly packed appearance. KLF17 depletion associated with reduced cell invasion (**C**) ($n = 3$; $^{**}P < 0.01$) and altered protein expression of EMT markers (**D**) as indicated. (**E**) HHUA cells described in (A) were incubated with paclitaxel for 24h and cell viability assay was performed ($n = 3$; $^{**}P < 0.01$). (**F**) Knockdown of KLF17 expression increases the proliferation of HHUA cells. (**G**) Colony number was shown ($n = 3$; $^{*}P < 0.05$).

KLF17 is a key regulator of the EMT/CSC gene network and other KLF members

To address the potential relationship of KLF17 with key transcription factors and signaling molecules implicated in EMT induction, we tried to determine whether KLF17 could affect the expression of known EMT/CSC-related genes in Ishikawa and HHUA cells by qRT–PCR. We found that the overexpression of KLF17 in Ishikawa cells dramatically increased endogenous mRNA levels of the EMT inducers *TWIST1*, *BMI-1* and oncogene *Id1* (28), moderately and significantly increased expression of *ZEB1*, *Snail* and *Slug*, and genes known to be involved in EMT (Figure 4A and Supplementary Figure S2A, available at *Carcinogenesis* Online). On the other hand, levels of the epithelial markers *E-cadherin* and *CK-18* were significantly reduced compared with control cells. Moreover, the mRNA levels of CSC markers (*NANOG*, *SOX2* and *CD133*), and chemoresistance-related genes (*MDR-1* and *MRP-1*) were also highly elevated in KLF17 vector-transfected cells. Interestingly, Ishikawa cells overexpressing KLF17 demonstrated increased levels of *KLF5* and *KLF13* and decreased *KLF9* expression. Consistent with these data, the KLF17-silenced HHUA cells showed remarkable downregulation of known EMT/CSC-promoting genes, *Id1* and *KLF13*, but upregulation of epithelial markers (*E-cadherin* and *CK-18*), and *KLF9* compared with control cells (Figure 4B and Supplementary Figure S2B, available at *Carcinogenesis* Online). These results indicate that KLF17 may control a network of genes involved in EMT and CSC and play a role in maintaining tumor growth and promoting tumor progression in EEC.

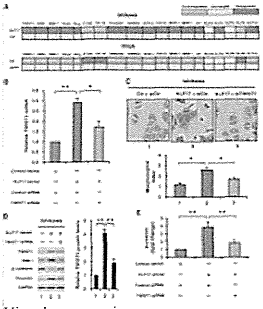

View larger version:

- In this window
- In a new window
- Download as PowerPoint Slide

Fig. 4.

TWIST1 is critical for KLF17-induced EMT and cell invasion. (**A**) The color-coded scale shows the relative mRNA expression of EMT/CSC-related genes and KLF family genes generated from qRT–PCRs using RNA from Ishikawa (up panel) and HHUA (bottom panel) cells expressing high or low KLF17 relative to the corresponding control cells, respectively. The red, gray, and green squares indicate upregulated, unchanged and downregulated transcripts, respectively. E-cad (E-cadherin). (**B**) Ishikawa cells transfected with control vector or KLF17 vector were transiently transfected with 20nM control siRNA (siCtr) or 20nM TWIST1 siRNA (siTWIST1). The mRNA levels of TWIST1 was analyzed by qRT–PCRs ($n = 3$; $^{*}P < 0.05$; $^{**}P < 0.01$; normalized to GAPDH). (**C**) Ishikawa cells described in (B) were stained with toluidine blue (up panel), and a quantitative analysis of cellular morphology (bottom panel) shows that the scattered morphology induced by KLF17 overexpression was partially reverted by TWIST1 silencing, resulting in a more round, cobblestone-like appearance. (**D**) Total protein extracts from cells described in (**B**) were immunoblotted as indicated antibodies. The semiquantitative analysis of TWIST1 and GAPDH was performed by computer-assisted densitometric scanning. (**E**) Downregulation of TWIST1 by specific siRNA reduced KLF17-mediated cell invasion ($n = 3$; $^{**}P < 0.01$).

TWIST1 is critical for KLF17-induced EMT and cell invasion

Because TWIST1 is essential for the induction of EMT (5) and upregulated in progressive endometrial cancer (29), and given our finding that KLF17 expression is positively correlated with that of TWIST1, we investigated as whether TWIST1 is a downstream target of KLF17 in promoting EMT in EEC cells. TWIST1 expression was increased in response to upregulation of KLF17 (Figure 4B and D) and decreased after knockdown of KLF17 (Figure 3D). We further silenced TWIST1 expression in Ishikawa cells overexpressing KLF17 by specific siRNA (Figure 4B and D) and found that downregulation of TWIST1 reduced KLF17-mediated cell invasion (Figure 4E). The scattered morphology induced by KLF17 overexpression was partially reverted by TWIST1 silencing, resulting in a more round, cobblestone-like appearance (Figure 4C, top panel). Transfection with TWIST1 siRNA, but not with control siRNA, significantly decreased the morphological index induced by KLF17 overexpression (Figure 4C, bottom panel). The reversal of the mesenchymal phenotype was confirmed by upregulation of epithelial marker E-cadherin and downregulation of EMT promoter BMI-1 and the mesenchymal marker Vimentin using immunoblotting (Figure 4D). These data suggest that TWIST1 is a critical downstream target of the KLF17-induced EMT signaling program that regulates the invasive properties of EEC cells.

KLF17 is a direct transcriptional activator of TWIST1

To test whether TWIST1 is target gene directly activated by KLF17 at the transcriptional level, a luciferase reporter driven by the reported *TWIST1* promoter (30) containing six potential KLF17-binding sequences (Figure 5A) was transfected in Ishikawa and HHUA cells together with KLF17 cDNA vector, KLF17 siRNA or controls. Reporter activity was induced upon overexpression of KLF17 (Figure 5B). In contrast, the opposite effects were observed following knockdown of KLF17 (Figure 5C), suggesting that KLF17 may act as transcriptional inducer of *TWIST1* via the recognition sites. To determine whether KLF17 binds the putative binding sites, we constructed point mutations of each site in the *TWIST1* promoter and performed luciferase assays. Mutagenesis of binding site F (–439/–435) reduced the luciferase activity of the TWIST1 pro-Luc construct, whereas mutation of other binding sites (A–E) did not significantly affect the luciferase activity (Figure 5D).

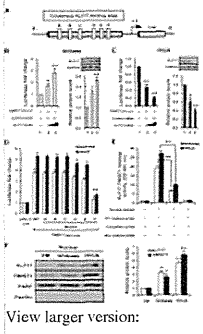

View larger version:

- In this window
- In a new window
- Download as PowerPoint Slide

Fig. 5.

KLF17 is a direct transcriptional activator of TWIST1. (**A**) Schematic representation of the *TWIST1* promoter with potential KLF17-binding sites. The luciferase construct driven from TWIST1 promoter was transfected in Ishikawa (**B**) or HHUA cells (**C**), together with KLF17 vector, KLF17 siRNA or their controls, respectively. Then the luciferase activities (left panel) was determined. The upregulation or downregulation of KLF17 was monitored by semiquantitative western blot (right panel) ($n = 3$; $^{*}P < 0.05$; $^{**}P < 0.01$). (**D**) Ishikawa and HHUA cells were transfected with a reporter gene construct containing either wild-type (WT) TWIST1 promoter, a similar promoter with mutated KLF17-binding sites (A–F) or a pGL3-Luc control vector. A luciferase assay was carried out ($n = 3$; $^{**}P < 0.01$). (**E**) Nuclear extracts from Ishikawa and HHUA cells were tested for KLF17 DNA-binding activity as measured by the transcription factor colorimetric assay ($n = 3$; $^{**}P < 0.01$). (**F**) Nuclear extracts from Ishikawa, HHUA and EM cells were subjected to semiquantitative western blot analysis of KLF17 and TWIST1. Purity of cytoplasmic or nuclear fractions was confirmed by immunoblotting the same blot with antibodies against paxillin (marker for cytoplasmic fraction) or PARP (marker for nuclear fraction), respectively.

To further characterize the interaction between KLF17- and the F-binding site, we quantified specific KLF17-binding activity on the consensus oligo using a transcription factor DNA-binding assay with a biotinylated capture probe spanning the –454 to –419 region of the *TWIST1* promoter. Nuclear extracts from Ishikawa and HHUA cells

exhibited complex formation with the consensus capture probe. Moreover, competition with unlabelled competitor probe significantly ablated the KLF17-*TWIST1* binding activity. No binding was detected between KLF17 and the oligonucleotides containing a mutated F site (Figure 5E). To further examine whether the increased expression of TWIST1 was a result of KLF17 transactivation, we measured the expression of KLF17 and TWIST1 in nuclear protein extracts from EEC cell lines and EM cells and we found that the nuclear KLF17 level correlated with the nuclear TWIST1 expression (Figure 5F), supporting a mechanistic and causal link between KLF17 and TWIST1 gene expression in ECs and the oncogenic role of KLF17 during EC metastasis. Together, these experiments support the model by which KLF17 directly binds to the *TWIST1* promoter to drive transactivation of the *TWIST1* gene in EEC cells, leading to EMT.

Elevated expression of KLF17 and TWIST1 in EECs

To address whether gain of KLF17 expression is an important event in endometrial carcinogenesis, we performed immunochemical analysis of KLF17 in 90 EECs and 18 benign endometrial samples. High KLF17 expression was found in 68% of EECs and in 39% of normal tissues (Figure 6A). KLF17 protein was predominantly located in the cytoplasm of the epithelial cells. We then investigated the possible correlation between KLF17 expression and clinical pathological characteristics in EECs. High KLF17 expression was detectable in 14 of 21 (60%) grade I EECs, 13 out of 44 (70%) grade II EECs and 9 out of 11 (82%) grade III EECs (Supplementary Table 1, available at *Carcinogenesis* Online), indicating that high KLF17 expression may correlate with increased tumor grade (Figure 6B). Increased KLF17 expression was also associated significantly with negative ER ($P = 0.002$), and marginally with PR status ($P = 0.053$) but not with other known prognostic markers (Supplementary Table 1, available at *Carcinogenesis* Online). Taken together, our data suggest that elevated expression of KLF17 is associated with advanced tumor grade and with the loss of steroid hormone receptors, both of which have been linked to EMT, tumor dedifferentiation and aggressive phenotypes of EEC (31–34).

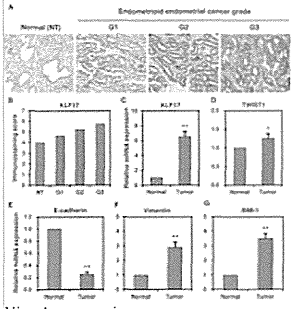

View larger version:

- In this window
- In a new window
- Download as PowerPoint Slide

Fig. 6.

Elevated expression of KLF17 and TWIST1 in EECs. (**A**) Immunochemistry of KLF17 in normal tissue (NT) and EEC. (**B**) High KLF17 expression correlated with increased tumor grade. Measurement of *KLF17* (**C**), *TWIST1* (**D**), *E-cadherin* (**E**), *Vimentin* (**F**) and *BMI-1* (**G**) mRNA expression in 24 pairs of EECs and their adjacent normal tissues was performed using qRT–PCRs, normalized to GAPDH. The data are means of triplicate measurements. Note the induced expression of *KLF17* and *TWIST*1 in EECs ($^{*}P < 0.05$; $^{**}P < 0.01$).

To further study the correlation of KLF17 levels with EMT-related gene expression in human EEC, we prepared RNA from EECs and adjacent normal tissues and determined the levels of *KLF17*, *TWIST1*, *BMI-1* and *Vimentin* and *E-cadherin* transcripts by qRT–PCR. Consistent with previous reports (9,35), EECs expressed significantly higher levels of *TWIST1*, *BMI-1* and *Vimentin* mRNA, and significantly lower levels of *E-cadherin* mRNA than benign tissues, paralleling the upregulation of *KLF17* transcripts (Figure 6C–G). These observation support the data derived from cell lines and strongly imply a role for KLF17 in upregulation of the expression of TWIST1 and subsequent induction of EMT during EEC cell invasion.

Discussion

In this study, we discovered a novel role for KLF17 in EEC progression via direct regulation of TWIST1. The KLF17 transcription factor is a member of the KLF family and has essential roles in human carcinogenesis through inhibition of EMT, tumor growth and invasion in human tumors (15–17). However, results of this study indicate that KLF17 can indeed function as a driver for EMT and that transactivation of TWIST1 plays a mechanistic role in KLF17-induced EMT and cell invasion in EEC cells. This is consistent with our finding of elevated expression of KLF17 in EEC tissues in which tumors are generally high grade and negative for ER and PR expression. Interestingly, previous work suggested that cancer cells isolated from high-grade EECs possess higher tumorigenic potential and stemness properties (36). In high-grade EECs showing more extensive myometrial invasion, loss of PR is strongly associated with increased expression of CD44 (a CSC marker) and decreased E-cadherin expression (34). These observations indicate that the molecular circuitries underlying EMT and cancer stemness may be closely intertwined during EEC progression. In agreement with this, we found that upregulation of KLF17 is involved in both promotion of cell invasion and increased resistance to paclitaxel *in vitro*, which raises a probability for a regulatory role of KLF17 in the enrichment of CSC of EEC *in vivo*.

The regulation of EMT involves complex signaling pathways including transforming growth factor-β, Wnt/β-catenin, Notch, and Hedgehog, which in turn activate major downstream transcription factors such as TWIST1, BMI-1, and others, leading to enhanced tumor invasion and metastasis (6,37,38). EMT has been recently linked to the acquisition of CSC properties and the progression of cancer, as evidenced by the ability of TWIST1-induced EMT to shift human epithelial cells to a more mesenchymal nature, with an increased expression of stem cell markers and acquisition of stem cell properties including proliferation and drug resistance (39). Our observation that KLF17 upregulates expression of either EMT-inducing transcription factors (*TWIST1*, *ZEB1*, *BMI-1*, *Snail* and *Slug*) or CSC-related genes (*NANOG*, *SOX-2*, *CD133*, *MDR-1* and *MRP-1*) indicates the possibility that KLF17 may function as an upstream mediator or a 'master switch' to facilitate the EMT-associated signaling networks (Supplementary Figure S3, available at *Carcinogenesis* Online). In agreement with this, all the transcription factors found to be regulated by KLF17 thus far are involved in EMT, deep myometrial invasion and the generation of CSC properties of EEC (35,36,40,41). Given the complexity of the signaling pathways that regulate EMT with formidable cross-talk and feedback (42), the mechanisms controlling KLF17 expression and the interactions between KLF17 and other EMT regulators should be fully elucidated.

Several signaling pathways such as scatter factor/hepatocyte growth factor-dependent pathways have been reported to activate or repress EMT in a cell type and context-dependent manner (43,44). These context-specific cellular effects of a given EMT regulator or pathway are ultimately controlled by the cooperative interaction between different signal pathways, epigenetic or genetic alterations of downstream genes, and the recruitment of other DNA-binding transcription factors or complexes to target gene promoters (45,46). Although KLF17 has been considered a key inhibitor of EMT and metastasis in breast cancer (15), our data suggest that KLF17 promotes EMT and EC cell invasion, providing the first evidence that KLF17 could function as cellular context-dependent transcriptional regulator to induce EMT in EC cells. It would be important to further identify its potential binding partners, effectors and downstream targets in ECs.

In addition, the function of KLFs, such as KLF5, as tumor suppressors or oncogenes may be dependent on p53 status (47). Considering that highly aggressive types of endometrial cancers frequently exhibit p53 mutations (48), it might be possible that in the presence of p53 mutation, distinct from its function in well-differentiated EECs, KLF17 exerts tumor-suppressor activity in poorly differentiated EECs to repress tumor progression. However, the precise role of KLF17 in invasive endometrial cancers

harboring p53 mutation remains to be further determined.

Conclusion

This study provides new insights into a potential mechanism of EEC invasion and progression mediated by KLF17 through TWIST1. Our data suggest that KLF17 overexpression is associated with EMT and tumor invasion by regulating TWIST1 and other EMT-related molecules.

Supplementary material

Supplementary Table 1 and Figures 1–3 can be found at http://carcin.oxfordjournals.org/

Funding

Department of Women's Health Educational System; a Grant-in-Aid from the Ministry of Health, Labour and Welfare of Japan; a Grant-in-Aid for Scientific Research (C) (23592428).

Conflict of Interest Statement: None declared.

Acknowledgement

We thank Dr Zhujie Xu for excellent technical assistance.

Abbreviations:

cDNA
: complementary DNA

CSC
: cancer stem cell

EEC
: endometrioid endometrial cancer

EMT
: epithelial–mesenchymal transition

ER
: estrogen receptor

IRS
: immunostaining score

KLF17
: Krüppel-like factor 17

mRNA
: messenger RNA

PBS
: phosphate-buffered saline

PCR
: polymerase chain reaction

PR
: progesterone receptor

qRT–PCR
: quantitative reverse transcription–polymerase chain reaction

shRNA
: short-hairpin RNA

siRNA
: small interfering RNA

WT
: wild-type.

References

1. Jemal A., et al . (2010) Cancer statistics, 2010. *CA. Cancer J. Clin.*, **60**, 277–300.
» Full-Text?@Hokkaido Univ. » CrossRef » Medline » Web of Science » Google Scholar

2. Ushijima K . (2009) Current status of gynecologic cancer in Japan. *J. Gynecol. Oncol.*, **20**, 67–71.
» Full-Text?@Hokkaido Univ. » CrossRef » Medline » Google Scholar

3. Endometrial Cancer-American Cancer Society. *What is endometrial cancer?*. http://www.cancer.org / (17 January 2013, date last accessed).

4. Amant F., et al . (2005) Endometrial cancer. *Lancet*, **366**, 491–505.
» Full-Text?@Hokkaido Univ. » CrossRef » Medline » Web of Science » Google Scholar

5. Weinberg R.A . (2008) Mechanisms of malignant progression. *Carcinogenesis*, **29**, 1092–1095.
» FREE Full Text

6. Shih J.Y., et al . (2011) The EMT regulator slug and lung carcinogenesis. *Carcinogenesis*, **32**, 1299–1304.
» Abstract/FREE Full Text

7. Yang M.H., et al . (2010) Bmi1 is essential in Twist1-induced epithelial-mesenchymal transition. *Nat. Cell Biol.*, **12**, 982–992.
» Full-Text?@Hokkaido Univ. » CrossRef » Medline » Web of Science » Google Scholar

8. Song L.B., et al . (2009) The polycomb group protein Bmi-1 represses the tumor suppressor PTEN and induces epithelial-mesenchymal transition in human nasopharyngeal epithelial cells. *J. Clin. Invest.*, **119**, 3626–3636.
» Full-Text?@Hokkaido Univ. » CrossRef » Medline » Web of Science » Google Scholar

9. Dong P., et al . (2011) MicroRNA-194 inhibits epithelial to mesenchymal transition of endometrial cancer cells by targeting oncogene BMI-1. *Mol. Cancer*, **10**, 99.
» Full-Text?@Hokkaido Univ. » CrossRef » Medline » Google Scholar

10. Dong P., et al . (2013) Mutant p53 gain-of-function induces epithelial-mesenchymal transition through modulation of the miR-130b-ZEB1 axis. *Oncogene*. **32**(27), 3286–3295. doi: 10.1038/onc.2012.334.
» Full-Text?@Hokkaido Univ. » CrossRef » Medline » Web of Science » Google Scholar

11. Yang Y., et al . (2005) KLF4 and KLF5 regulate proliferation, apoptosis and invasion in esophageal cancer cells. *Cancer Biol. Ther.*, **4**, 1216–1221.
» Full-Text?@Hokkaido Univ. » CrossRef » Medline » Web of Science » Google Scholar

12. Nandan M.O., et al . (2004) Krüppel-like factor 5 mediates the transforming activity of oncogenic H-Ras. *Oncogene*, **23**, 3404–3413.
» Full-Text?@Hokkaido Univ. » CrossRef » Medline » Web of Science » Google Scholar

13. Yu F., et al . (2011) Kruppel-like factor 4 (KLF4) is required for maintenance of breast cancer stem cells and for cell migration and invasion. *Oncogene*, **30**, 2161–2172.
» Full-Text?@Hokkaido Univ. » CrossRef » Medline » Web of Science » Google Scholar

14. Simmons C.D., et al . (2011) Krüppel-like factor 9 loss-of-expression in human endometrial carcinoma links altered expression of growth-regulatory genes with aberrant proliferative response to estrogen. *Biol. Reprod.*, **85**, 378–385.
» Abstract/FREE Full Text

15. Gumireddy K., et al . (2009) KLF17 is a negative regulator of epithelial-mesenchymal transition and metastasis in breast cancer. *Nat. Cell Biol.*, **11**, 1297–1304.
» Full-Text?@Hokkaido Univ. » CrossRef » Medline » Web of Science » Google Scholar

16. Cai X.D., et al . (2012) Reduced expression of Krüppel-like factor 17 is related to tumor growth and poor prognosis in lung adenocarcinoma. *Biochem. Biophys. Res. Commun.*, **418**, 67–73.
» Full-Text?@Hokkaido Univ. » CrossRef » Medline » Google Scholar

17. Liu F.Y., et al . (2013) Down-regulated KLF17 expression is associated with tumor invasion and poor prognosis in hepatocellular carcinoma. *Med. Oncol.*, **30**, 425.
» Full-Text?@Hokkaido Univ. » CrossRef » Medline » Google Scholar

18. Matsushima-Nishiu M., et al . (2001) Growth and gene expression profile analyses of endometrial cancer cells expressing exogenous PTEN. *Cancer Res.*, **61**, 3741–3749.
» Abstract/FREE Full Text

19. Kyo S., et al . (2003) Successful immortalization of endometrial glandular cells with normal structural and functional characteristics. *Am. J. Pathol.*, **163**, 2259–2269.
» Full-Text?@Hokkaido Univ. » CrossRef » Medline » Web of Science » Google Scholar

20. Mori N., et al . (2010) Expression of HER-2 affects patient survival and paclitaxel sensitivity in endometrial cancer. *Br. J. Cancer*, **103**, 889–898.
» Full-Text?@Hokkaido Univ. » CrossRef » Medline » Web of Science » Google Scholar

21. Dong P., et al . (2009) Elevated expression of p53 gain-of-function mutation R175H in endometrial cancer cells can increase the invasive phenotypes by activation of the EGFR/PI3K/AKT pathway. *Mol. Cancer*, **8**, 103.
» Full-Text?@Hokkaido Univ. » CrossRef » Medline » Google Scholar

22. Haynes J., et al . (2011) Dynamic actin remodeling during epithelial-mesenchymal transition depends on increased moesin expression. *Mol. Biol. Cell*, **22**, 4750–4764.
» Abstract/FREE Full Text

23. Dong P.X., et al . (2008) Silencing of IQGAP1 by shRNA inhibits the invasion of ovarian carcinoma HO-8910PM cells *in vitro* . *J. Exp. Clin. Cancer Res.*, **27**, 77.
» Full-Text?@Hokkaido Univ. » CrossRef » Medline » Google Scholar

24. Truty M.J., et al . (2009) Silencing of the transforming growth factor-beta (TGFbeta) receptor II by Kruppel-like factor 14 underscores the importance of a negative feedback mechanism in TGFbeta signaling. *J. Biol. Chem.*, **284**, 6291–6300.
» Abstract/FREE Full Text

25. Scholten A.N., et al . (2006) Combined E-cadherin, alpha-catenin, and beta-catenin expression is a favorable prognostic factor in endometrial carcinoma. *Int. J. Gynecol. Cancer*, **16**, 1379–1385.
» Full-Text?@Hokkaido Univ. » CrossRef » Medline » Google Scholar

26. Peng C., et al . (2012) Expression and prognostic significance of wnt7a in human endometrial carcinoma. *Obstet. Gynecol. Int.*, **2012**, 134962–134970.
» Full-Text?@Hokkaido Univ. » Medline » Google Scholar

27. Mani S.A., et al . (2008) The epithelial-mesenchymal transition generates cells with properties of stem cells. *Cell*, **133**, 704–715.
» Full-Text?@Hokkaido Univ. » CrossRef » Medline » Web of Science » Google Scholar

28. Takai N., et al . (2001) Id1 expression is associated with histological grade and invasive behavior in endometrial carcinoma. *Cancer Lett.*, **165**, 185–193.
» Full-Text?@Hokkaido Univ. » CrossRef » Medline » Web of Science » Google Scholar

29. van der Horst P.H., et al . (2012) Progesterone inhibits epithelial-to-mesenchymal transition in endometrial cancer. *PLoS One*, **7**, e30840.
» Full-Text?@Hokkaido Univ. » CrossRef » Medline » Google Scholar

30. Cheng G.Z., et al . (2008) Twist is transcriptionally induced by activation of STAT3 and mediates STAT3 oncogenic function. *J. Biol. Chem.*, **283**, 14665–14673.
» Abstract/FREE Full Text

31. Oreskovic S., et al . (2004) A significance of immunohistochemical determination of steroid receptors, cell proliferation factor Ki-67 and protein p53 in endometrial carcinoma. *Gynecol. Oncol.*, **93**, 34–40.
» Full-Text?@Hokkaido Univ. » CrossRef » Medline » Google Scholar

32. Sivridis E., et al . (2001) Endometrial carcinoma: association of steroid hormone receptor expression with low angiogenesis and bcl-2 expression. *Virchows Arch.*, **438**, 470–477.
» Full-Text?@Hokkaido Univ. » CrossRef » Medline » Web of Science » Google Scholar

33. Wik E., et al . (2013) Lack of estrogen receptor-α is associated with epithelial-mesenchymal transition and PI3K alterations in endometrial carcinoma. *Clin. Cancer Res.*, **19**, 1094–1105.
» Abstract/FREE Full Text

34. Hanekamp E.E., et al . (2003) Consequences of loss of progesterone receptor expression in development of invasive endometrial cancer. *Clin. Cancer Res.*, **9**, 4190–4199.
» Abstract/FREE Full Text

35. Montserrat N., et al . (2012) Epithelial to mesenchymal transition in early stage endometrioid endometrial carcinoma. *Hum. Pathol.*, **43**, 632–643.
» Full-Text?@Hokkaido Univ. » CrossRef » Medline » Google Scholar

36. Hubbard S.A., et al . (2009) Evidence for cancer stem cells in human endometrial carcinoma. *Cancer Res.*, **69**, 8241–8248.
» Abstract/FREE Full Text

37. Bailey J.M., et al . (2007) Cancer metastasis facilitated by developmental pathways: Sonic hedgehog, Notch, and bone morphogenic proteins. *J. Cell. Biochem.*, **102**, 829–839.
» Full-Text?@Hokkaido Univ. » CrossRef » Medline » Web of Science » Google Scholar

38. Katsuno Y., et al . (2013) TGF-β signaling and epithelial-mesenchymal transition in cancer progression. *Curr. Opin. Oncol.*, **25**, 76–84.
» Full-Text?@Hokkaido Univ. » CrossRef » Medline » Google Scholar

39. Floor S., et al . (2011) Cancer cells in epithelial-to-mesenchymal transition and tumor-propagating-cancer stem cells: distinct, overlapping or same populations. *Oncogene*, **30**, 4609–4621.
» Full-Text?@Hokkaido Univ. » CrossRef » Medline » Web of Science » Google Scholar

40. Kyo S., et al . (2006) High Twist expression is involved in infiltrative endometrial cancer and affects patient survival. *Hum. Pathol.*, **37**, 431–438.
» Full-Text?@Hokkaido Univ. » CrossRef » Medline » Web of Science » Google Scholar

41. Tsukamoto H., et al . (2007) Irradiation-induced epithelial-mesenchymal transition (EMT) related to invasive potential in endometrial carcinoma cells. *Gynecol. Oncol.*, **107**, 500–504.
» Full-Text?@Hokkaido Univ. » CrossRef » Medline » Google Scholar

42. Thiery J.P., et al . (2006) Complex networks orchestrate epithelial-mesenchymal transitions. *Nat. Rev. Mol. Cell Biol.*, **7**, 131–142.
» Full-Text?@Hokkaido Univ. » CrossRef » Medline » Web of Science » Google Scholar

43. Zavadil J., et al . (2005) TGF-beta and epithelial-to-mesenchymal transitions. *Oncogene*, **24**, 5764–5774.
» Full-Text?@Hokkaido Univ. » CrossRef » Medline » Web of Science » Google Scholar

44. Polyak K., et al . (2009) Transitions between epithelial and mesenchymal states: acquisition of malignant and stem cell traits. *Nat. Rev. Cancer*, **9**, 265–273.
» Full-Text?@Hokkaido Univ. » CrossRef » Medline » Web of Science » Google Scholar

45. Ikushima H., et al . (2010) Cellular context-dependent "colors" of transforming growth factor-beta signaling. *Cancer Sci.*, **101**, 306–312.
» Full-Text?@Hokkaido Univ. » CrossRef » Medline » Google Scholar

46. Meier-Stiegen F., et al . (2010) Activated Notch1 target genes during embryonic cell differentiation depend on the cellular context and include lineage determinants and inhibitors. *PLoS One*, **5**, e11481.
» Full-Text?@Hokkaido Univ. » CrossRef » Medline » Google Scholar

47. Yang Y., et al . (2012) p53 mutation alters the effect of the esophageal tumor suppressor KLF5 on keratinocyte proliferation. *Cell Cycle*, **11**, 4033–4039.
» Full-Text?@Hokkaido Univ. » CrossRef » Medline » Web of Science » Google Scholar

48. Matias-Guiu X., et al . (2013) Molecular pathology of endometrial carcinoma. *Histopathology*, **62**, 111–123.
» Full-Text?@Hokkaido Univ. » CrossRef » Medline » Web of Science » Google Scholar

« Previous | Next Article » Table of Contents

This Article

1. *Carcinogenesis (2014) 35 (4): 760-768. doi: 10.1093/carcin/bgt369* First published online: November 11, 2013

1. AbstractFree
2. » Full Text (HTML)Free
3. Full Text (PDF)Free
4. Supplementary Data
5. All Versions of this Article:
    1. bgt369v1
    2. bgt369v2
    3. 35/4/760 most recent

Classifications

1. ◦ Original Manuscript

Services

1. Alert me when cited
2. Alert me if corrected
3. Find similar articles
4. Similar articles in Web of Science
5. Similar articles in PubMed
6. Add to my archive
7. Download citation
8. Request Permissions

Citing Articles

1. Load citing article information
2. Citing articles via CrossRef
3. Citing articles via Scopus
4. Citing articles via Web of Science
5. Citing articles via Google Scholar

Google Scholar

1. Articles by Dong, P.
2. Articles by Sakuragi, N.
3. Search for related content

PubMed

Online ISSN 1460-2180 - Print ISSN 0143-3334

Eur J Nucl Med Mol Imaging (2014) 41:446–451
DOI 10.1007/s00259-013-2610-9

ORIGINAL ARTICLE

Impact of FDG PET in optimizing patient selection for cytoreductive surgery in recurrent ovarian cancer

Yasuhiko Ebina · Hidemichi Watari · Masanori Kaneuchi · Mahito Takeda · Masayoshi Hosaka · Masataka Kudo · Hideto Yamada · Noriaki Sakuragi

Received: 19 June 2013 / Accepted: 7 October 2013 / Published online: 13 November 2013

Abstract
Purpose To investigate the impact of PET and PET/CT scanning on decision-making in management planning and to identify the optimal setting for selecting candidates for surgery in suspicious recurrent ovarian cancer.
Methods A retrospective chart review was performed in patients with possible recurrent ovarian cancer after primary optimal cytoreduction and taxane/carboplatin chemotherapy who had undergone FDG PET or FDG PET/CT scans from July 2002 to August 2008 to help make treatment decisions. The analysis included 44 patients who had undergone a total of 89 PET scans. The positive PET scans were classified as follows. (1) localized (one or two localized sites of FDG uptake), (2) multiple (three or more sites of FDG uptake), (3) diffuse (extensive low-grade activity outlining serosal and peritoneal surfaces).
Results Of the 89 PET scans, 52 (58.4 %) led to a change in management plan. The total number of patients in whom cytoreductive surgery was selected as the treatment of choice increased from 12 to 35. Miliary disseminated disease, which was not detected by PET scan, was found in 22.2 % of those receiving surgery. Miliary disseminated disease was detected in 6 of the 12 patients with recurrent disease whose treatment-free interval (TFI) was <12 months, whereas none of those with a TFI of ≥12 months had such disease (P=0.0031).
Conclusion PET or PET/CT is useful for selecting candidates for cytoreductive surgery among patients with recurrent ovarian cancer. To avoid surgical attempts in those with miliary dissemination, patients with a TFI of ≥12 months are the best candidates for cytoreductive surgery.

Keywords Ovarian cancer · Recurrence · Cytoreduction · FDG PET

Y. Ebina (✉) · H. Yamada
Department of Obstetrics and Gynecology, Kobe University Graduate School of Medicine, Kobe 650-0017, Japan
e-mail: ebiyas@med.kobe-u.ac.jp

H. Watari · M. Kaneuchi · M. Takeda · M. Hosaka · M. Kudo · N. Sakuragi
Department of Gynecology, Hokkaido University Graduate School of Medicine, Sapporo 060-8638, Japan

Introduction

The majority of women with advanced ovarian cancer eventually develop recurrent disease despite achieving a clinical complete remission after initial treatment. With few exceptions, recurrent ovarian cancer patients are unlikely to be cured of their disease. Thus the goal of treatment is to improve the quality of life and lengthen the survival period. Most patients are offered further chemotherapy, although the response is limited. The role of secondary cytoreductive surgery for recurrent ovarian cancer is still controversial.

Several studies have found factors associated with outcome in patients who have undergone secondary cytoreductive surgery. The treatment-free interval (TFI) prior to secondary cytoreductive surgery and residual disease after it have been demonstrated to be associated with better outcome [1, 2]. However, the ratio of patients with optimal resection is as low as 70 % [3]. This might be due to the difficulty in predicting the possibility of attaining optimal cytoreduction. The proper preoperative selection of candidates remains unclear. The purposes of this study were to investigate the impact of PET scan findings (e.g. FDG uptake patterns) on decision making for management planning and to identify the optimal setting for selecting candidates for surgery from among those with suspicion of recurrent ovarian cancer.

Patients and methods

After obtaining Institutional Review Board approval, a retrospective chart review was performed in patients with possible recurrent ovarian cancer who had undergone FDG PET or FDG PET/CT scans between July 2002 and August 2008 at Hokkaido University Hospital. This analysis included 44 patients who had undergone a total of 89 PET scans (60 FDG PET, 29 FDG PET/CT) during this period. All patients had histologically confirmed ovarian cancer and underwent primary optimal cytoreduction and taxane/carboplatin chemotherapy.

The images were reviewed by radiologists with experience in CT and nuclear medicine physicians with experience in PET. Whole-body ^{18}F-FDG PET imaging was performed using an ECAT EXACT 47 scanner (Siemens-CTI, Knoxville, TN). Before the PET study, all of the patients fasted for at least 6 h, and serum glucose levels were checked before administration of ^{18}F-FDG. The dose of ^{18}F-FDG was 185 MBq in each patient. Static emission scans were performed 60 min after ^{18}F-FDG administration using the three-dimensional acquisition mode with a duration of 2 min per bed position. PET/CT imaging was performed using a Discovery LS system (GE Medical Systems, Milwaukee, WI). Patients fasted for a minimum of 4 h prior to PET acquisition. After confirmation of a blood glucose level <200 mg/dl, sterile FDG was administered intravenously (4.5 MBq/kg) followed by a tracer uptake phase of approximately 70 min. Positron emission data were acquired for five to seven bed positions, typically from the base of the skull to the mid-thigh. Emission data were acquired for 3 min for each bed position. PET images were reconstructed using the CT data for attenuation correction using the 2-D OSEM algorithm. The CT portion of the Discovery LS consisted of a multidetector helical CT scanner. Imaging parameters were as follows for an acquisition with five bed positions: 140 mA, 60 mA, 0.6 s per CT rotation.

The standard surveillance protocol for patients with ovarian cancer consists of physical examination and evaluation of serum CA 125 levels at intervals of 2 to about 3 months for the initial 24 months after completion of primary therapy and every 4 months thereafter. Abdominal and chest contrast-enhanced CT scans are performed every 6 months. Patients with an increased serum CA 125 (20 U/ml or more) and a negative or equivocal CT scan receive a PET scan. The presence, region and pattern (e.g. nodular, diffuse) of FDG uptake are fully reviewed. A management plan is then discussed. Close observation is recommended for patients who do not have distinct accumulation on PET scans despite an increased CA 125. Systemic chemotherapy is given in patients who show a multiple or diffuse FDG uptake pattern. Otherwise, cytoreductive surgery is proactively considered in patients whose FDG uptake patterns are localized.

The positive PET scans were classified into three categories of FDG uptake pattern: (1) localized (one or two localized sites of FDG uptake, (2) multiple (three or more sites of FDG uptake, each site with nodular uptake), (3) diffuse (extensive low-grade activity outlining serosal and peritoneal surfaces). TFI was defined as the time from completion of initial treatment or any previous recurrent treatment to the time of latest recurrence.

Statistical analyses were carried out using Statistica software (StatSoft, Tulsa, OK). Correlations among the variables were analysed using Fisher's exact test and the chi-squared test. The Kruskal-Wallis test was used for nonparametric variables. $P<0.05$ was considered statistically significant.

Results

The analysis included 44 patients who had undergone a total of 89 FDG PET scans (20 patients had one scan, 12 patients had two scans, and 12 patients had three or more scans). The indications for PET scanning were abnormal CT findings (48.3 %), a rise in serum CA 125 (37.1 %), suspicion of relapse on physical examination (10.1 %), or clinical symptoms (4.5 %). Most patients (95.5 %) were asymptomatic at the time of the PET scan. Detailed characteristics of the patients are shown in Table 1. The majority of patients had stage III (65.9 %) and grade 3 (63.7 %) disease at initial

Table 1 Characteristics of the patients who had PET or PET/CT to evaluate localization of recurrent ovarian cancer

Characteristic	Value
Age at initial diagnosis (years), median (range)	54.5 (31 – 74)
Stage at initial diagnosis, *n* (%)	
I	4 (9.1)
II	6 (13.6)
III	29 (65.9)
IV	5 (11.4)
Tumour grade, *n* (%)	
1	6 (13.6)
2	10 (22.7)
3	28 (63.7)
Histology, *n* (%)	
Serous	30 (68.2)
Clear	7(15.9)
Endometrioid	4(9.1)
Other	3(6.8)
Number of scans, *n* (%)	
1	20 (45.4)
2	12 (27.3)
>3	12 (27.3)

diagnosis. Most patients had serous histology (68.2 %). The management plans before and after PET in relation to the FDG uptake patterns are shown in Fig. 1. Of the scans showing positive FDG uptake, 46 (51.7 %) were classified as showing localized uptake, 18 (20.2 %) as showing multiple uptake, and 18 (20.2 %) as showing diffuse uptake. In total, 58.4 % of PET scans (52/89) led to a change in the patient's management plan. After the PET scan, the total number of candidates in whom surgery was planned increased from 12 to 35 (35 of 89; 39.3 %).

Table 2 shows the FDG uptake pattern in relation to the TFI in 82 patients in whom positive FDG uptake was detected. The proportions of patients with a localized pattern with TFI <3 months, 3 to <6 months, 6 to <12 months, and ≥12 months were 36.0 %, 52.9 %, 58.8 % and 78.3 %, respectively. A significantly greater proportion of patients with a TFI ≥6 months had a localized uptake pattern than those with a TFI <6 months (70.0 % vs. 42.9 %; $P=0.012$). In patients with serous histology, the relationship between serum CA 125 level and FDG uptake pattern was examined. The proportion of patients with a localized FDG uptake pattern decreased as the CA 125 level increased: 77.8 % (14/18) in those with CA 125 ≤50 U/ml, 66.7 % (10/15) in those with CA 125 50 to ≤100 U/ml, and 41.4 % (12/29) in those with CA 125 >100 U/ml ($P=0.038$).

A total of 35 cytoreductive operations were performed in 25 patients. The median patient age was 60 years (range 35 – 78 years). The histological types were: serous in 68 % of patients, clear cell in 20 %, endometrioid in 8 % and mucinous in 4 %. The initial FIGO stages were: I in 12 % of patients, II in 12 %, III in 56 % and IV in 20 %. The tumour grades were: 1 in 24 % of patients, 2 in 20 % and 3 in 56 %. The median TFI prior to cytoreductive surgery was 10 months (range 1 – 70 months). The surgical procedures are listed in Table 3. The results of the cytoreductive operations are shown in Table 4. In all patients, recurrent tumours preoperatively detected on PET scans were recognized during surgery. No macroscopic tumours that were undetectable on preoperative PET scans were discovered during surgery. However, 22.2 % (6/27) of patients exhibited miliary disease in the abdominal cavity that could not be detected by PET. The TFIs in the patients who had miliary disseminated disease were 6, 6, 6, 7, 8 and 10 months. In addition, a small to modest amount of ascites (<500 ml) was found during surgery in 11.1 % of these patients (3/27) that was not seen preoperatively. All the patients with ascites had miliary disease. Macroscopically complete resection was achieved in 91.4 % of cytoreduction procedures (32/35). On the other hand, following 3 of the 35 procedures (8.6 %), the patient had residual tumour less than 0.5 cm in diameter, and these were the patients who had miliary disease on the peritoneal surface. There were no patients who had residual tumours measuring more than 0.5 cm. Pathological examination confirmed recurrent disease in all patients. The median tumour diameter was 30 mm (range 10 – 72 mm). The mean estimated blood loss was 80 ml (range 10 – 580 ml). The median operative time was 125 min (range 50 – 450 min). There were no severe postoperative complications.

Regarding the 27 intraperitoneal operations, the factors that were related to peritoneal miliary dissemination are shown in Table 5. Miliary dissemination was detected in 6 (50.0 %) of the 12 patients with a TFI <12 months, compared with none of those with a TFI ≥12 months ($P=0.0031$). Miliary dissemination was detected in 3 (12.5 %) of the 24 patients with no

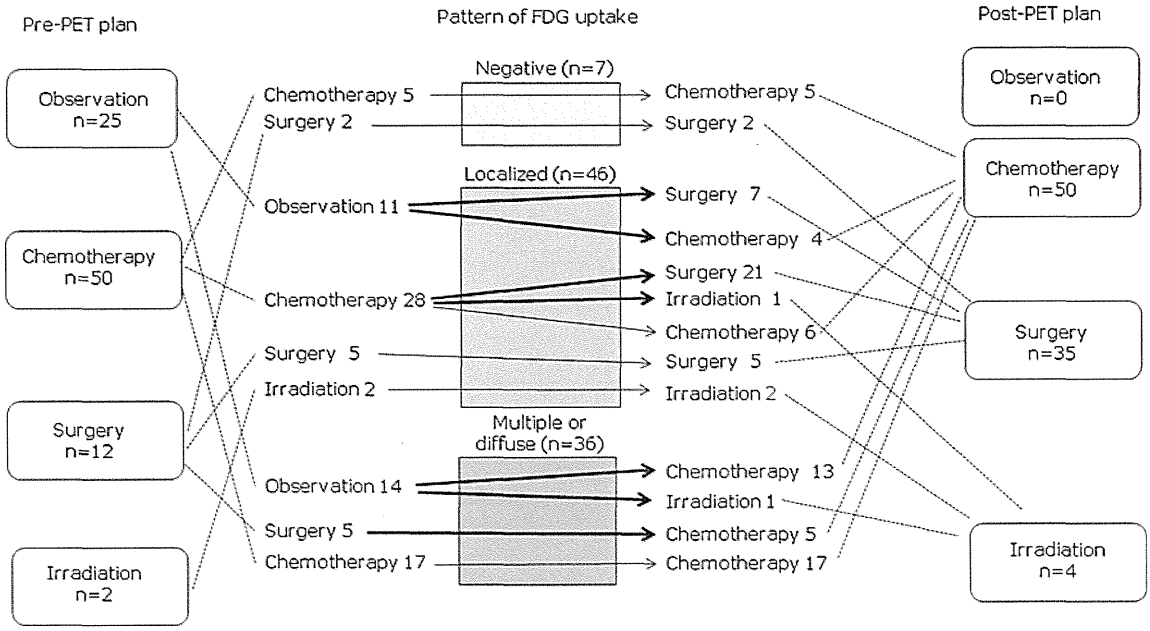

Fig. 1 Treatment plans before and after PET in patients with suspected recurrent ovarian cancer

Table 2 The association between TFI and FDG uptake pattern

TFI (months)	No. of patients			*P* value
	Total	Localized pattern	Multiple or diffuse pattern	
<3	25	9 (36.0 %)	16 (64.0 %)	
3 to <6	17	9 (52.9 %)	0 (47.1 %)	
6 to <12	17	10 (58.0 %)	7 (41.2 %)	
≥12	23	18 (78.3 %)	5 (21.7 %)	
<6	42	18 (42.9 %)	24 (57.1 %)	0.012[a]
≥6	40	28 (70.0 %)	12 (30 %)	

[a] Comparing uptake pattern between patients with a TFI <6 months and those with a TFI ≥6 months

ascites during the operation, in contrast to this finding in all three patients with measurable ascites ($P=0.0068$). In addition to these variables, none of the other variables analysed (secondary, tertiary or quaternary cytoreduction, serous or other, grade 1/2 or 3, CA125 <100 U/ml or ≥100 U/ml, one or two recurrent lesions, size of maximum tumour <30 mm or ≥30 mm) predicted miliary disease.

Discussion

In this study, 58 % of PET scans led to a change in the management of the patient. PET scanning was especially useful in selecting candidates for site-specific treatment (e.g. surgery, irradiation). Cytoreductive surgery had a high the rate of complete resection (91 %). Even if a PET scan indicates localized disease, patients with a TFI of ≥12 months are the best candidates for complete resection due to the tumour size limitation. For optimal management in recurrent ovarian cancer, it is necessary to consider the following factors: length of the TFI/platinum-free interval, possible second-line regimens, prior adverse effects experienced by the patient, and patient choice. Several studies have demonstrated that an elevation of serum CA 125 can precede the appearance of clinically or radiographically measurable recurrence by an average of 3 to 6 months [4, 5]. However, early retreatment in asymptomatic patients is still controversial. OV05/EORTC 55955 trials have concluded that there is no survival benefit from early treatment based on an elevated serum CA 125 level alone [6]. On the contrary, investigators have recently reported that the

Table 3 Surgical procedures used in the treatment of recurrent ovarian cancer

Procedure	Number
Tumour cytoreduction alone	6
Bowel resection	9
Rectal resection	3[a]
Other large-bowel resection	4
Small-bowel resection	2
Hepatic resection	5
Splenectomy	3
Distal pancreatectomy	1
Diaphragm resection	3
Cholecystectomy	1
Para-aortic node dissection	3
Cervical node dissectIon	3
Axillary node dissection	2
Inguinal node dissection	1
Video-assisted thoracoscopic surgery	2
Chest wall resection	1
Upper vaginectomy	1
Partial cystectomy	1

[a] Colostomy 2

Table 4 Results of cytoreductive surgery for recurrent ovarian cancer

Characteristic	Value
Age at cytoreduction (years), median (range)	60 (35 – 78)
Secondary cytoreduction, *n* (%)	24 (68.5)
Tertiary cytoreduction, *n* (%)	8 (22.9)
Quaternary cytoreduction, *n* (%)	3 (8.6)
Treatment-free interval (months), median (range)	10 (1 – 70)
Number of recurrent lesions, *n* (%)	
1	27 (77.1)
2	8 (22.9)
Size of largest recurrence (mm), median (range)	30 (10 – 72)
Dissemination, *n* (%)	
Yes	6 (22.2)
No	21 (77.8)
Ascites at operation, *n* (%)	
Yes	3 (11.1)
No	24 (88.9)
Residual tumour, *n* (%)	
No gross	32 (91.4)
<0.5 cm	3 (8.6)
>0.5 cm	0 (0.0)
Operation time (mm), median (range)	125 (50 – 450)
Bleeding in operation (g), median (range)	80 (10 – 580)